The ScaRaB Earth Radiation Budget Dataset

R. Kandel,* M. Viollier,* P. Raberanto,* J. Ph. Duvel,* L. A. Pakhomov,+ V. A. Golovko,+ A. P. Trishchenko,#,& J. Mueller,@ E. Raschke,@ R. Stuhlmann,@ and the International ScaRaB Scientific Working Group (ISSWG)

ABSTRACT

Following an overview of the scientific objectives and organization of the French–Russian–German Scanner for Radiation Budget (ScaRaB) project, brief descriptions of the instrument, its ground calibration, and in-flight operating and calibration procedures are given. During the year (24 February 1994–6 March 1995) of ScaRaB Flight Model 1 operation on board *Meteor-3/7*, radiometer performance was generally good and well understood. Accuracy of the radiances is estimated to be better than 1% in the longwave and 2% in the shortwave domains. Data processing procedures are described and shown to be compatible with those used for the National Aeronautics and Space Administration's (NASA) Earth Radiation Budget Experiment (ERBE) scanner data, even though time sampling properties of the *Meteor-3* orbit differ considerably from the ERBE system orbits. The resulting monthly mean earth radiation budget distributions exhibit no global bias when compared to ERBE results, but they do reveal interesting strong regional differences. The "ERBE-like" scientific data products are now available to the general scientific research community. Prospects for combining data from ScaRaB Flight Model 2 (to fly on board *Ressurs-1* beginning in spring 1998) with data from the NASA Clouds and the Earth's Radiant Energy System (CERES) instrument on board the Tropical Rainfall Measurement Mission (TRMM) are briefly discussed.

1. Introduction

a. The ScaRaB-1 mission

The Scanner for Radiation Budget (ScaRaB) project is a cooperative project of France, Russia, and Germany. The first ScaRaB flight model (FM1) was integrated on the Russian operational weather satellite *Meteor-3/7* and launched on 24 January 1994 from the Plesetsk spaceport in northwest Russia. Earth observations began on 24 February 1994 and continued (with some interruptions) until 6 March 1995 when the instrument failed. The instrument, described in section 2 below (cf. also Monge et al. 1991; Kandel et al. 1994a), measured reflected and emitted radiances in four channels (visible, solar, total, infrared window); these data have been processed to yield broadband shortwave (SW) and longwave (LW) fluxes, for all-sky and clear-sky scenes, on the same spatial and temporal scales as the ERBE [National Aeronautics and Space Administration's (NASA) Earth Radiation Budget Experiment] products (Barkstrom et al. 1989). Following examination by participating project members and the International ScaRaB Scientific Working Group (ISSWG; see Table 1), a set of ScaRaB-1 products has been judged to be sufficiently "validated" to be made available to the broader scientific community for further study and scientific use (available upon request from scarab@cst.cnes.fr). Here, following a

*Laboratoire de Météorologie Dynamique, Centre National de la Recherche Scientifique, Palaiseau, France.
+Scientific Research Center for Exploration of Natural Resources Dolgoprudny, Russia.
#Research Institute for Hydrometeorological Information, Obninsk, Russia.
@Institute for Atmospheric Physics, GKSS Research Center, Geesthacht, Germany.
&Current affiliation: Canada Centre for Remote Sensing, Ottawa, Ontario, Canada.
Corresponding author address: Dr. Robert Kandel, Laboratoire de Météorologie Dynamique du CNRS, Ecole Polytechnique, F-91128 Palaiseau, Cedex, France.
E-mail: Kandel@lmd.polytechnique.fr
In final form 5 January 1998.

TABLE 1. The International ScaRaB Scientific Working Group (ISSWG).

Participating institution/ original project partners	Principal investigator, co-PIs, co-Is
CNRS–Laboratoire de Météorologie Dynamique (BRC+instrument teams), Ecole Polytechnique, Palaiseau, France	R. Kandel, M. Capderou, J. Ph. Duvel, P. Raberanto, F. Raison, F. Sirou, C. Stubenrauch, M. Viollier
Scientific Research Center for the Study of Natural Resources, Moscow, Russia	L. A. Pakhomov, V. A. Golovko, A. B. Uspensky
Research Inst. on Hydrometeorological Information, Obninsk, Russia	R. G. Reitenbach, A. N. Trotsenko (Kurchatov Inst., Moscow), A. P. Trishchenko (now at CCRS, Ottawa, Canada)
Inst. for Atmospheric Physics, GKSS Research Centre, Geesthacht, Germany	R. Stuhlmann, E. Raschke, J. Mueller, H. Leighton (McGill University, Montreal)
CNES–Centre Spatial de Toulouse, France	J. Roussel, Th. Trémas, H. Marquier, J.-F. Fronton
ISSWG partners	
California Space Inst., University of California, La Jolla, California	W. Collins (now at NCAR, Boulder, Colorado)
Canada Centre for Remote Sensing, Ottawa, Canada	A. P. Trishchenko, Z. Li
CNRS–Laboratoire de Météorologie Dynamique (ARA team), Ecole Polytechnique, Palaiseau, France	F. Cheruy, N. A. Scott
CNRS–Laboratoire de Météorologie Dynamique, BRC and MDC teams, Palaiseau and Paris, France	J.-P. Duvel, S. Bony, M. Capderou, R. Kandel, H. Le Treut, C. Stubenrauch, M. Viollier
CNRS–Laboratoire d'Optique Atmosphérique, Univ. Sci. Techn. de Lille, France	F. Parol, J. C. Buriez, Y. Fouquart, M. Vesperini
Hadley Centre for Climate Prediction and Research, Meteorological Office, Bracknell, United Kingdom	A. Slingo, J. A. Pamment, M. J. Webb, J. E. Harries [Imperial Coll. London (ICL)], A. Sinha (ICL), K. P. Shine (University of Reading)
Inst. of Atmos. Sci., South Dakota School of Mines and Technology, Rapid City, South Dakota	S. A. Christopher, R. M. Welch (now at University of Alabama in Huntsville, Huntsville, Mississippi)
KMI–IRM (Royal Meteorological Institute), Brussels, Belgium	D. Crommelynck, J. Cornelis (VUB), P. Boekaerts (VUB), M. Acheroy (ERM)
NASA/Goddard Institute for Space Studies, New York, New York	A. A. Lacis, B. E. Carlson, W. B. Rossow
NASA/Langley Research Center, Hampton, Virginia	G. L. Smith (Virginia Polytechnic Inst.), E. F. Harrison, R. B. Lee III, T. P. Charlock, P. Minnis
Saratov State University, Saratov, Russia	Yu. A. Sklyarov, D. I. Trubetskov
Satellite Research Laboratory, Hungarian Met. Serv., Budapest, Hungary	G. Major, I. Csiszar, M. Putsay, A. Rimoczi-Paal, A. Merza
Voeikov Main Geophysical Observatory, Saint Petersburg, Tsvetkov, Russia	G. G. Shchukin, O. M. Pokrovsky, A. V. Tsvetkov

brief review of the scientific problems to which such data are relevant, we present an overview of the 1-yr ScaRaB-1 data product set. In particular, we describe the instrument (section 2) and its performance and calibration (section 3) so that prospective users will be aware of the potential problems in the data. In section 4 we evaluate to what extent the ScaRaB processing from pixel radiances to monthly regional mean fluxes is consistent with procedures used in ERBE, and the uncertainties that affect different data products. In section 5 we survey the salient features of the ScaRaB-1 results, comparing them to the ERBE record. In the final section, we consider prospects for continuing and improved radiation budget measurements from ScaRaB-2, CERES (Clouds and the Earth's Radiant Energy System), and other projected missions.

b. Earth radiation budget observations for climate research

The planetary radiation budget has always been a key parameter of interest for climate research, as a measure of the energy exchanges between the planet Earth and space and for the forcing or atmospheric and ocean circulation systems. Early estimates (cf. Hunt et al. 1986) were based on conventional climatological data and also on the earthshine on the moon. Later analyses used data from the first and second generations of meteorological satellites and from the NASA Nimbus missions (cf., e.g., Raschke et al. 1973; Stephens et al. 1981; Jacobowitz et al. 1984; House et al. 1986). All energy exchange of significance between the earth–atmosphere system and its cosmic environment is radiative (cf., e.g., Kandel 1990). The system absorbs part of the incoming solar SW radiation flux and reemits this energy flux to space in degraded LW form with a spectrum characteristic of temperatures in the 200–300-K range. Reflected solar SW radiation flux, with a spectrum extending roughly from 0.2 to 5 μm, ranges from zero to 1000 W m^{-2} locally and instantaneously. The earth–atmosphere system emits LW thermal radiation over wavelengths mostly greater than 3.3 μm; outgoing LW flux ranges from 120 to 450 W m^{-2} with a global annual mean value of 238 W m^{-2}. Reflected SW and emitted LW spectra are fairly distinct, although there is overlap during daytime at wavelengths between 3.3 and 5 μm, where radiative flux density is relatively low for both spectra.

The distribution of top of atmosphere (TOA) net radiation (radiation balance, equal to absorbed SW minus emitted LW fluxes) defines the energy sources/sinks that drive the general circulation of the atmosphere and oceans but is at the same time a consequence of the general circulation. The absorbed (incident – reflected) solar SW radiation gives the (mostly) externally imposed radiative forcing of the system. The annual cycle of the global mean TOA net radiation has a reasonably well-determined peak-to-peak amplitude of approximately 15 W m^{-2}, with maximum positive values occurring in late Southern Hemisphere summer. The nonzero values (a few watts per square meter) of the annual average global mean TOA net radiation found from ERBE and ScaRaB data are an indication of observational uncertainty rather than of global radiative imbalance. The geographic distribution of the LW flux emitted to space (also called outgoing longwave radiation) provides useful information on the overall state of the surface–atmosphere column. Important progress has been made in establishing the climatology of these quantities, thanks in particular to the Nimbus/ERB (Earth Radiation Budget) and the ERBE missions of NASA, but sampling problems continue to limit accuracy. Strong biases remain likely, especially, but not only, in the shortwave fluxes. Because these biases depend on the particular orbit–instrument combination and SW absolute calibration, and because TOA ERB components are vertically integrated quantities, detection of global climate trends in the ERB is probably illusory. However, observations of ERB changes during major climate anomalies [El Niño–Southern Oscillation (ENSO) events, major volcanic eruptions, etc.] are essential to test the realism of climate simulations.

The last ERBE scanner ceased operation on 28 February 1990. Data from the wide-field-of-view (WFOV) nonscanner instrument on board the *Earth Radiation Budget Satellite* (*ERBS*) continued to provide calibrated broadband data, but ERB components with spatial resolution finer than 500–1000 km could only be derived using multispectral narrowband satellite imagery. Therefore, the ScaRaB-1 data came just in time to partially bridge the gap before the next long-term time series of calibrated broadband moderate spatial resolution data expected from the CERES missions.

The so-called cloud radiative forcing (CRF; cf. Charlock and Ramanathan 1985) can be computed as a model product. Observational estimates of CRF require spatial resolution finer than 100 km in order to measure clear-sky radiances. These estimates provide needed constraints on models, many of which otherwise may appear to be right for the wrong reasons; indeed, correct all-sky ERB distribution are obtained with many models that exhibit radically different cloud

radiative effects, most of which must be wrong (Cess and Potter 1987; Cess et al. 1990).

There exist many publications (cf. Kandel 1990; Wielicki et al. 1995) based on the 5-yr ERBE scanner data record and the continuing stream of ERBE WFOV data. The study of the recent radiation budget history with data on cloud radiative forcing (Ramanathan et al. 1989) has led to important new insights into the functioning of the "clear-sky greenhouse effect" (Raval and Ramanathan 1989; Stephens and Greenwald 1991a; Bony and Duvel 1994; Bony et al. 1995) and the influence of clouds (Stephens and Greenwald 1991b; Sohn and Robertson 1993). Unfortunately, observations of climate shocks ("natural experiments") such as the 1991 Pinatubo eruption (Minnis et al. 1993), and of large-scale climate anomalies such as the prolonged 1990–95 ENSO event (Trenberth and Hoar 1996), have with few exceptions (such as the 1986–87 ENSO) been limited to a combination of coarse spatial resolution broadband measurements (ERBE/WFOV) and uncalibrated narrowband data [National Oceanic and Atmospheric Administration/Advanced Very High Resolution Radiometer (NOAA/AVHRR)]. Therefore, although detection of climate trends may be uncertain or impossible using TOA ERB data only, new and continuing observations of broadband ERB components remain essential to accurate characterization of ERB variability and anomalies. Here we consider the broadband scanner data furnished by ScaRaB-1 operating on broad *Meteor-3/7* (Viollier et al. 1997). We expect new broadband scanner observations from CERES on the Tropical Rainfall Measurement Mission (TRMM) launched in November 1997, ScaRaB-2 on Ressurs, to be launched in spring 1998, and launches of CERES on EOS-AM in 1998 and EOS-PM in 2000 (Wielicki et al. 1996). With these new data, the TOA ERB climatology can be extended to include a broader sample of climate anomalies.

2. The ScaRaB project and instrument

a. The project

The ScaRaB project was initiated in 1986 in the framework of what was then the French–Soviet Cooperation for Space Research. Germany joined the project in 1988. ScaRaB became the joint responsibility of France, Russia, and Germany early in 1992. The original aim was to provide broadband observations of the ERB with spatial resolution adequate for estimation of cloud radiative forcing, in particular but not solely in order to ensure continuity of coverage after NASA/ERBE scanner operation ended and well before the start of NASA/CERES scanner observations (cf. Stowe 1988). In fact, the ERBE scanner on board *ERBS* operated successfully for over 5 yr, until 28 February 1990; the first of the CERES scanners was launched on board the NASA–NASDA TRMM satellite in November 1997. Thus ScaRaB-1, which operated between February 1994 and March 1995, filled only a part of the gap. Note that polar regions cannot be observed from either *ERBS* or TRMM; ScaRaB-1 partly filled a gap in polar narrow-field-of-view coverage that otherwise would extend nearly 10 yr from May 1989 (failure of the ERBE scanner on board *NOAA-10*) to mid-1998 (launch of EOS-AM with CERES).

b. The satellite platform

ScaRaB FM1 observed from the Russian *Meteor-3/7* weather satellite. The orbit of this satellite was circular at an altitude of 1200 km and polar with an inclination of 82.5°. With such a prograde orbit, the satellite was *not* sun synchronous; the orbit plane precessed relative to the sun–earth vector with a period of approximately 213 days (cf. Capderou 1995). This provides full coverage of the diurnal cycle in about 106 days, so that monthly mean products can be biased by the convolution of diurnal and interdiurnal variations. In particular, shortwave flux estimates for some months are based on near-terminator (low sun) measurements.

c. The instrument

The instrument is composed of a scanning module and an onboard calibration module, together with necessary electronics including memory for up to 14 h of data.

1) The scanning module

ScaRaB is a four-channel cross-track scanning radiometer with angular resolution 48 mrad. Scanning is obtained by rotation of a cylinder (the rotor) carrying the optics, filters, detector, choppers, and analog-detection electronics about an axis parallel to the direction of motion of the spacecraft, within a cylinder (stator) mounted on the spacecraft. The four channels (Table 2) include two broad spectral bands from which the reflected SW and emitted LW radiances are derived and two narrower bands similar to operational weather satellite imager channels, one corresponding to the infrared atmospheric window, the other to the visible (green to red) portion of the solar spectrum. The lower 0.2-μm limit of SW and total radiation (TW)

channel response corresponds to the cutoff in reflectance of the aluminum mirror optics. There is no abrupt longwave cutoff in spectral response of the TW channel although a gradual fall in response is expected as wavelengths become comparable to paint thickness. Even if response *were* zero at all wavelengths beyond 50 μm, assuming it to remain constant instead would lead to an error of 1–2 W m^{-2} sr^{-1} for earth-emitted "unfiltered'' (i.e., spectrally corrected) LW radiances between 40 and 150 W m^{-2} sr^{-1}. In the absence of reliable spectral response measurements beyond 50 μm, we have assumed a continuation of the falloff observed between 20 and 50 μm, and we estimate the maximum resulting error in unfiltered LW radiance to be less than 1%.

TABLE 2. ScaRaB channels.

Channel no.	Description	Wavelength range	Filter type
1	Visible (VIS)	0.55–0.65 μm	Interference
2	Solar (SW)	0.2–4 μm	Fused silica
3	Total (TW)	0.2–50 μm	Unfiltered
4	IR window (IRW)	10.5–12.5 μm	Interference

The instrument has been described earlier (Monge et al. 1991; Kandel et al. 1994a), but we give a summary description in what follows. We also summarize principal differences between ScaRaB and the ERBE scanner in Table 3.

Daytime radiation in the LW band (nominally 4–50 μm) is determined by appropriately weighted subtraction of the SW signal from the TW signal. Possible differences or variations in SW spectral response of the SW and TW channels can lead to errors in filtered and unfiltered daytime LW radiances, but analysis (Raison 1996) indicates that these are smaller than 1%. Note that although the ERBE scanner had an LW channel, the unfiltered LW radiances were in practice determined from such TW–SW subtraction (cf. Thomas et al. 1995; Green and Avis 1996). Determination of LW radiances by the CERES scanner will also use spectral subtraction.

Each channel is a small telescope with a spherical aluminum mirror focusing incoming radiation directly onto the detector at the prime focus, with no secondary reflection. Each optical system is centered so as to be insensitive to polarization. The four channels are mounted in parallel inside the rotor cylinder, perpendicular to its axis. The field of view is defined by a square field stop, whose diagonal is parallel to the scan direction. Half-diagonal overlapping of pixels reduces aliasing. For ScaRaB FM1, which flew on *Meteor-3/7* at 1200-km altitude, the projection on the ground, at nadir, of the instantaneous field of view (pixel) is a 60-km square, with pixel spacing on a square grid of 42.5 km.

The detectors are windowless pyroelectrics coated with black paint. The radiation arriving on each detector is chopped at the pixel sampling frequency. Each of the two choppers is a rotating hemispherical mirror with two openings; each detector alternately receives radiation transmitted directly from outside and radiation reflected from a small internal "reference blackbody." This is not a calibration source; its temperature is not actively controlled. The temperature of the reference blackbody for channel 3 is measured by a platinum resistance thermometric sonde and included

TABLE 3. Principal ERBE NFOV–ScaRaB differences.

ScaRaB	ERBE
Cross-track scanning only	Azimuth of scanning plan variable
Detector at prime focus (one reflection)	Cassegrain system (two reflections)
Pyroelectric detectors	Thermistor bolometers
Slowly changing instrument temperature	Active thermal control
Each pixel chopped	No chopping
Space look every 6 s	Space look every 4 s
Two broadbands (SW, TW); two narrow bands	Three broad bands (SW, TW, LW)
Special filtered calibration modes	Mirror attenuator mosaic for SW calibration
Frequent calibrations (12 s, 24 min)	Less frequent calibrations
Fixed calibration blackbody temperature	Possibility to vary blackbody temperature

in the scientific telemetry. These data and thermal modeling of the instrument confirm that these temperatures are stable on timescales as long as several scan cycles (Raison 1996).

The pixel signal is the difference between the signal integrated (for 20 ms) when the chopper is fully open to the external scene and the signal obtained when it is fully closed and reflecting the internal blackbody. The only differences in the channels are the filters present or absent (for TW) in the optical path. Note that because the filters used for channels 1, 2, and 4 are located between the chopper and the detector, their thermal emission is eliminated. Radiometer bias is canceled using a space look at the beginning or end of each scan line (depending on the direction of the sun, which is avoided). It may be noted that the CERES instrument is similar to the ERBE scanner, but with the imperfect broad LW band replaced by an infrared window channel (8–13 μm) analogous to but somewhat broader than ScaRaB IRW channel 4 (10.5–12.5 μm).

2) The onboard calibration module

The onboard calibration sources are housed in a module *external* to the scanning module. They include two high quality blackbodies (distinct from the small internal blackbodies) viewed by the TW and infrared window (IRW) channels 3 and 4 every other scan, that is, every 12 s. Temperature of these blackbodies was actively controlled at 310 K and accurately monitored by a platinum temperature sonde implanted in the blackbody. Blackbody emissivity was 0.993 in channel 3 and 0.995 in channel 4.

For the SW domain, the calibration system was designed with three sets of calibration lamp sources. This system did not work as planned on FM1, but with more careful preaging of lamps, it is hoped that it will work on FM2. The sources include 1) incandescent lamp sources L22 and L23 designed to be used to compare the response of SW channel 2 with the SW response of the TW channel 3; 2) additional lamp sources L11 and L12 used to monitor the visible and SW channels 1 and 2; and 3) lamp sources L32 and L33 used as a further check on the stability of L22 and L23. The lamp source pair L22–L23 consists in fact of two intermingled bundles of optical fibers illuminated by two incandescent lamps; by design the output brightness ratio should remain constant even if one or the other input lamp drifts. On FM1, failure of one of the lamps of source L22–L23 led to an in-flight ratio inconsistent with preflight calibrations, and gains in the SW channel and the SW portion of the TW channel were interpolated between calibration modes (see below). The L22/L23 ratio deduced from these gains was, however, found to remain fairly constant (to 5%) through the mission.

d. Modes of operation

The scan cycle is of 6-s duration. In-flight operation modes include earth measurement modes and calibration modes.

1) Earth measurement modes

This mode includes an earth scan over about 100°, a space look on the antisolar side of the instrument, and measurements of the onboard external calibration sources. Successive scans include measurements of the external blackbodies for the TW and IRW channels and of two lamp sources (L22 and L23) for the SW and TW channels. The external blackbody views yield gain of the IRW channel and the LW portion of the TW channel every 12 s. For channel 2 and the SW portion of channel 3, the position of L22–L23 was viewed every other scan, but in order to conserve lifetime the lamp source pair was switched on only five times during each orbit. For channel 3, thermal radiation from L23 was taken into account using views with L23 switched off. On ScaRaB FM2, these measurements are to be used to monitor possible variations of the gains of the SW channel and the SW portion of the TW channel and to compare these with the LW gains of the TW channel determined by blackbody views every 12 s. Offsets are known every 6 s from the space views.

2) Calibration modes

In calibration modes a few tens of 6-s scan cycles (288 or 480 s total) are devoted to views of external calibration sources not observed during the earth measurement modes. With modes E1–E2, which occur only twice per 24-h period, and E4 (twice per month), lamp sources L11–L12 and L32–L33 are used, together with various filters, to check SW–TW gain balance, stability of the more frequently used lamps, and spectral response within the bands.

e. Ground calibration

Ground calibrations of FM1 and the engineering model were performed at two different facilities. Scanner characterization and calibration of the onboard blackbody simulators were carried out in a vacuum chamber at the Institut d'Astrophysique Spatiale in Orsay, France. Onboard shortwave sources for ScaRaB Engineering Model and FM1 were cali-

brated at the solar tower operated by the German Kiepenheuer-Institut at the Observatorio del Teide (28.3°N, 16.5°W, altitude 2370 m; Tenerife, Canary Islands, Spain). For FM2 and FM3, solar calibration was carried out at Odeillo in southwest France.

In the IAS vacuum chamber, ScaRaB (with temperature controlled at values between +5° and +35°C) observed a cold blackbody (−50°C) located in front of the space view port and a hot blackbody (up to +60°C) with actively controlled temperature placed at different positions inside the ±50° earth field of view. These two blackbodies have in-axis emissivity of 0.9998. Temperatures were measured with platinum resistance thermometers calibrated by the Physikalisch-Technische Bundesanstalt (Germany) between 10° and 80°C, and by the Laboratoire National d'Essais (France) from −50° to 0°C. Important points established were (i) linearity of response, (ii) no variation of gains and offsets with position in the field of view, (iii) no influence on neighboring pixels of a bright object in the scan field, and (iv) onboard lamp source radiances independent of the air/vacuum condition. These operations yielded radiometric calibration of the temperature and emissivity of the onboard calibration blackbodies and calibration of the temperature dependence of detector gains.

For the solar ground calibration, the calibration standard is a reference diffusor, illuminated by the sun. Simultaneously, the incoming solar irradiance is measured by a calibrated pyrheliometer, and the relative solar spectral distribution is measured by a spectrometer. ScaRaB, the diffusor/baffle assembly, the pyrheliometer, the spectrometer, and ancillary instruments are mounted in the Ground Calibration Unit (GCU) built by Sensorlab (Munich). At Tenerife the GCU was mounted on an equatorial table, maintaining the alignment between the common line of sight of the instruments and the sun. The calibration procedures and results have been described by Mueller et al. (1993), Mueller et al. (1996), and Mueller et al. (1997). Accuracy of the ground calibrations of the onboard blackbodies is estimated to be 0.4%; of the onboard lamp sources, better than 1.5%.

3. Flight model 1 in-flight performance and calibration

Data were received from February 1994 to March 1995, with a few interruptions of instrumental or satellite origin (Table 4). Instrument temperatures generally remained between 7° and 37°C. Long-term behavior in large part followed the changing orbital configuration over the lifetime of the instrument; over shorter periods, various instrument temperatures underwent cycling with the orbital period (110 min) and amplitudes of 0.5° to 2°C (Raison and Kandel 1995; Raison 1996). In addition to this cycling, internal instrument temperatures rose as much as 1.5°C during calibration modes (every 12 h), the rise being followed by a relaxation over the next few thousand seconds. This behavior has been modeled and is explained by the heat released by the internal filter wheel motor that operates during such modes (Raison 1996).

Temperatures of the external calibration module blackbodies for the TW and IRW channels 3 and 4 were effectively maintained at +37.00°C within 0.01°C. The gains determined from the blackbody views of each of these two channels, every 12 s, are fixed functions of detector temperature measured in channel 3. The comparison of gains established from blackbody calibration and those calculated from the detector temperature showed agreement within 0.1%. Nevertheless, the overall uncertainty in LW calibration is higher, due to possible uncontrolled variations of instrument parameters and of the radiometer environment. Comparing the results for different calibration modes and ground testing, we believe the accuracy of nighttime LW calibration to be close to the 0.4% level of the ground calibration (Mueller et al. 1997). Although departures from linearity could not be checked in flight, the ground calibration results, together with modeling of the detection process (Raison 1996) and arguments of internal consistency, lead us

TABLE 4. ScaRaB Flight Model 1 history.

Activity or anomaly	Date(s)
Launch of *Meteor-3/7* at Plesetsk	25 January 1994
Start of earth observations	24 February 1994
Noisy space views	April 1994: data recovered
Loss of satellite telemetry, followed by filter wheel blockage	30 September–9 November 1994: nearly all data lost
Scanner failure	6 March 1995

to believe that response remained linear throughout the mission. Considering also the above-cited uncertainty in far-IR spectral response, we believe calibration accuracy in the LW domain is better than 1%.

Because of partial failure of L22–L23, it was necessary to establish the SW gain during measurement mode by interpolation between biweekly E4 calibration modes. The assumptions that SW gain is a single linear function of detector temperature and that absolute brightness of calibration source L32 was constant throughout flight operations yielded consistent results, with precise reproducibility of several thermal cycles in these measurements during radiometer lifetime. Although there is no assurance that absolute brightness of L32 did not change between ground calibration and flight, in-flight SW calibration is estimated to be reliable at the 1% level as analyzed by Dinguirard and Trémas (1997) and Trishchenko and Li (1998). Analysis of desert targets (Capderou 1997) confirms the accuracy and stability of SW radiance determinations from March 1994 to February 1995. The SW/TW gain balance, important for determining daytime LW radiances, appears to have remained constant to better than 1% (Raison 1996); the balance parameter was determined using the SW, TW, and IRW channel data and a method analogous to that applied by Thomas et al. (1995) to ERBE data. Also, analysis of very cold bright daytime cloud scenes over tropical convective regimes, for which the TW signal is dominated by SW reflection and the LW component can be estimated independently from the IRW radiance, yields agreement at the 1% level (J. P. Duvel 1997, personal communication).

ScaRaB data for March 1994 have been compared with ERBE nonscanner observations from ERBS for near-simultaneous collected views, using the ERBE angular models to convert ScaRab flux estimates into radiances contributing to the ERBE WFOV signal (Bess et al. 1997). Considering the numerous uncertainties in this procedure, especially in angular modeling (see also section 4a below), the agreement is excellent. The mean differences (0.8 and 3.8 W m^{-2} for SW and daytime LW, respectively, nighttime LW differences being smaller) and the corresponding standard deviations (5.5 and 2.3 W m^{-2} are comparable to those between fluxes derived from ERBE scanner and nonscanner data (Green et al. 1990).

Data from all four ScaRaB channels (both broadband and the narrower VIS and IRW channels) for April and July 1994 have also been compared to *GOES-7* datasets generated within the Atmospheric Radiation Measurement Program. Using the most recent version of GOES datasets, agreement with ScaRaB observations was found to be better than 2% on average for narrowband and broadband albedos and within 5 W m^{-2} for LW and SW fluxes. (Li and Trishchenko 1998; Trishchenko and Li 1998; Doelling et al. 1998). Such consistency tends to increase our confidence in the ScaRaB calibration, because otherwise one must believe that the independent ScaRaB and GOES instruments and procedures have the same biases.

4. From instantaneous pixel radiances to monthly regional mean fluxes

a. Spectral and angular corrections

One of the keys to the determination of the Earth Radiation Budget is the "scene identification." It is a major parameter in all steps of the processing: spectral corrections, radiance-to-flux conversion, time–space averaging, and cloud radiative forcing calculation. To minimize biases between ERBE and ScaRaB time series, the same 12 scene classifications as ERBE (Smith et al. 1986) are used, based on the combination of five geotypes (ocean, land, snow–ice, desert, coast) and four cloud categories (clear, partly cloudy, mostly cloudy, overcast). The algorithm of scene identification is the maximum likelihood estimation (MLE; Wielicki and Green 1989), which compares the measured (unfiltered) LW and SW radiances to a predefined set of radiances for the appropriate geometry of view and geographic zone (Suttles et al. 1988a; Suttles et al. 1988b). The algorithm is adjusted to account for regional variations of clear-sky surface albedos and for diurnal as well as regional variations of LW fluxes of land and desert geotypes.

The raw radiances are first corrected for spectral filtering effects, as a function of the identified scene. The ScaRaB FM1 response is not perfectly flat and diminishes substantially at wavelengths below 0.4 μm. Using the simulation of reflected SW radiances for 530 cases, Viollier et al. (1995) were unable to find a monotonic spectral correction function of cloud cover. However, for clear and partly cloudy ocean scenes, a correction of +5% significantly reduces the spectral filtering errors (standard deviation 1.2 W m^{-2} for the 530 cases). Although one might expect a smaller nonzero correction to apply to mostly cloudy ocean scenes, this was not confirmed by the calculation, and no correction is introduced. Clear and partly cloudy ocean

scenes appear blue from space, but the white reflection of clouds overwhelms the blue in a mostly cloudy scene.

The second correction based on the scene identification is the angular correction, more precisely the use of an anisotropic factor for radiance-to-flux conversion. The ERBE angular models (Suttles et al. 1988) have been used here to ensure consistency between ERBE and ScaRaB products. For a future version, new angular LW corrections have been defined using the ScaRaB infrared window channel 4 (Stubenrauch et al. 1993), new SW corrections have been computed for desert scenes using Meteosat data (Capderou 1997), and others are under development using POLDER/ADEOS data (Deschamps et al. 1994). The CERES team also is developing new broadband angular models for an expanded set of scene types, using both existing *Nimbus-7*/ERB and ERBE data, and expected multiangular views from the CERES scanner pairs to fly on the EOS-AM and EOS-PM platforms (Suttles et al. 1992; Wielicki et al. 1996). It should be remembered that SW angular corrections may be greater than a factor of 4 and are the major source of uncertainty for instantaneous and daily mean SW flux estimates.

b. Space and time averaging

The first steps of the processing were done at the pixel level. The remaining computations deal with space averages of the elementary observations over geographical areas of $2.5° \times 2.5°$ latitude and longitude. These averages, called instantaneous regional means, are collected for an entire month and region by region.

Time sampling is another important issue for ERB determination. Indeed, except at high latitude, a satellite in a near-polar orbit observes a particular region only twice a day. Two observations (one in the SW) are not sufficient to account for the diurnal variations of the earth surface–atmosphere system, which are related to variations of temperature and cloudiness driven by the daily cycle of insolation. The instantaneous regional means are interpolated or extrapolated along the day to all local times (values at the local half hour, e.g., 0030, 0130, etc.) using the same algorithms as ERBE (Brooks et al. 1986). In the LW domain, the radiant flux interpolation is linear over ocean and snow–ice but uses a daytime half-sine fit over land/desert and coastal scenes. In the SW domain, each regional instantaneous average is adjusted to the local half hours, taking into account modeled directional albedo for each scene type and differences of sun elevation. Region by region, the estimated local hourly radiant fluxes are then averaged to compute the daily means, the monthly means of the diurnal variation, and the overall monthly means.

c. Error sources

Sources of error are numerous at all steps of the processing. Individual misclassification of scenes can result in erroneous angular corrections (cf., e.g., Ye and Coakley 1996), and indeed, even if the scene classification is correct, angular correction uses a model (in particular a bidirectional reflectance distribution function in the SW) that is valid at best only statistically. Incomplete sampling of diurnal variations also can have a large impact. The final steps of the processing involve combining many pixel observations to produce quasi-instantaneous spatial mean values and then interpolating and averaging them over time. If one assumes the individual observations to be statistically independent, the error in the regional and global means (resulting from processing 5×10^7 elementary measurements) should be considerably reduced. In the case of two-satellite ERBE data, rms uncertainties have been estimated at 3 and 5 W m^{-2}, respectively, for the longwave and shortwave monthly regional average fluxes (Harrison et al. 1990).

However, the individual observations are not always statistically independent, and the sampling of viewing and illumination angles and of local time is not uniform. The errors in the individual pixel fluxes are therefore not always random, and they may persist in the regional means. With regard to time-averaged quantities, one must distinguish regions where the extent and properties of clouds undergo pronounced systematic and coherent diurnal variations (e.g., Duvel 1988). In a broad sense, low-level clouds (stratus, stratocumulus, etc.) have maximum extent in the morning along the eastern boundary currents over ocean, whereas high-level clouds associated with deep convection tend to occur more often in the late afternoon and evening over the continents. Time sampling of such systematic variations may be incomplete, leading to bias in the daily and monthly mean radiation budget components. Other systematic errors occur when a sun-synchronous satellite is observed only in the early morning and late afternoon: the LW maximum arising from maximum surface temperature at or after midday over land and desert is systematically erased.

Additional complexity affects the interpretation of ScaRaB/Meteor results due to the orbital precession

period of 213 days. All local hours are observed only after about 106 days (considering both ascending and descending sides of the orbit) and each month has then a different and restricted time coverage. Four months (end of March–April 1994, July 1994, November 1994, and February 1995) are more specifically biased, since they are observed in near-terminator conditions (as for ERBE on *NOAA-10*). Daily and monthly means of LW fluxes are affected by such sampling to the extent that the midday maximum of LW emission is missed. With additional modeled diurnal variations for cloud-free and partly cloudy land and desert regions, Viollier et al. (1997) found that underestimation up to 6 W m^{-2} may occur for certain desert regions in these near-terminator months. The daily and monthly mean SW and net fluxes depend on extrapolation of an albedo determined from a low-sun observation. The directional model used for such extrapolation is itself uncertain and gives high leverage to any SW measurement error. The results for the near-terminator months (especially November 1994, for which the first 10 days are missing) therefore have higher uncertainty than for other months.

Clear-sky calculations face other problems. In many land regions with strong nighttime surface cooling, the ERBE MLE often misidentifies the nighttime scene as cloudy, so that regional instantaneous clear-sky LW flux is obtained with very few pixels or is missing. The ScaRaB undersampling due to both the pixel size and the one-satellite coverage eliminates most of the nighttime values with low fluxes from the clear-sky record. The interpolation algorithm then takes mainly into account the higher daytime fluxes and the monthly value may be slightly overestimated. To prevent such errors, we apply more severe conditions to obtain clear-sky determination: LW regional monthly means are not computed when there are fewer than three daytime observations of the region in the month.

Studies under development are testing the ability to correct time-sampling bias with the incorporation of data from geostationary satellites (Duvel and Kandel 1985; Cheruy et al. 1991; Rieland and Raschke 1991; Kandel et al. 1994b; Haeffelin et al. 1998; Standfuss 1997). Together with possible improvement of scene identification (Briand et al. 1998) and angular models (Stubenrauch et al. 1993; Capderou 1997), this should lead to a new version of the secondary data processing and a second release of the dataset. At present the whole set of ScaRaB data products has been provided to ISSWG principal investigators in the ERBE-like version described above. These products are further described in the following section.

d. ScaRaB-1 science data products

There are three levels of science data products, described in Table 5. The first two levels (A1, A2) are organized in daily files containing quantities relevant to each pixel in order of observation, A2 being directly comparable to the ERBE Processed Archival Tapes (PAT or S-8). The third level (A3) is organized in monthly files, with quantities (spatial averages, other statistics) given for the ERBE 2.5° × 2.5° latitude–longitude regions. The four subsets of the A3 level correspond to different degrees of temporal averaging.

5. Results obtained from Flight Model 1

Results (Figs. 1–5) are shown in color maps on a Mollweide equal-area projection (using GMT software; Wessel and Smith 1991). The equal-angle grid of the ScaRaB computation is first resampled using simple weighted averages of neighboring points. This yields a slight smoothing and a sensible reduction of the no-data areas where clear skies are not observed over an extended time period. A linear interpolation is also used to fill the latitude bands where the sun was too low to allow reliable computation of the reflected SW flux, which in such a case must be small.

a. Outgoing longwave flux

Regional longwave fluxes are shown in Fig. 1 for March, June, September, and December 1994. In a broad sense the highest values corresponding to the highest LW fluxes at the top of the atmosphere are observed for cloud-free areas over the highest-temperature surfaces: tropical oceans and deserts. On the contrary the lowest values (in blue and purple) correspond to the highest optically thick clouds, that is, to deep convection in the intertropical convergence zone (ITCZ) near the equator and to clouds or ice-covered surfaces in the polar zones.

The same determination of outgoing longwave flux is carried out separately selecting only measurements identified as clear sky (Fig. 2). Values range from more than 280 W m^{-2} in the cloud-free parts of the intertropical zone, to as low as 140 and 180 W m^{-2}, respectively, over Antarctica and Greenland. The no-data areas are those where clear-sky days were not identified by the ERBE algorithms and where the neighboring-pixel resampling technique failed. Note that all cloud radia-

TABLE 5. ScaRaB science data products.

	ERBE analog	Organization	Description—quantities included
A1	"pre-PAT"	Daily files, pixel by pixel as observed	Geographical location, instrument counts, housekeeping data, calibration data, filtered radiances each channel, for each pixel
A2	PAT S-8	Daily files, pixel by pixel as observed	Geographical location, illumination/viewing geometry, filtered radiances each channel, scene identification, unfiltered SW, LW radiances, SW and LW fluxes
A3	S-9	Monthly files, ERBE regions	Regional mean quantities and other statistics
A3 MRI	Record-2	ERBE regions, by satellite overpass	Quasi-instantaneous regional means: all-sky and clear-sky SW and LW fluxes, other statistics, scene-type fractions
A3 MRJ	Part of record 1	ERBE regions, day by day	As above, daily regional means
A3 MRH	Part of record 1	ERBE regions, hour by hour	Monthly hourly regional means, that is, monthly mean diurnal variation of above quantities
A3 MRMJ	Part of record 1	ERBE regions	Monthly regional means obtained from daily regional means
A3 MRMH	Part of record 1	ERBE regions	Monthly regional means obtained from monthly hourly regional means

tive forcing maps based on radiometric estimates of clear-sky as well as all-sky fluxes are sensitive to details of the interpolation procedure in areas where cloud occurrence is close to 100%.

b. Reflected shortwave flux and albedo

The all-sky and clear-sky albedos are shown, respectively, in Figs. 3 and 4. Albedo is undefined during polar night (gray areas on the June and December maps). The clear-sky maps are the easiest to interpret. The main interseasonal change is due to the ice–snow cover (albedo higher than 45%), with a very large extent over northern Asia and North America in December and March. The same is observed in the south with maximum sea-ice extent during June and July. Other bright regions (albedo between 20% and 40%) are deserts, with maxima in Sahara and Arabia. Albedo increase with solar zenith angle is observed over deserts as well as over oceans. Of course, cloud contamination as well as high ocean surface roughness (wave height) may also contribute to this increase. Elsewhere the variations are small and probably meaningless, showing the limits of the data processing. Isolated patterns over oceans probably reflect the difficulty to correctly detect partial cloud cover and carry out radiance-to-flux conversion. Except for such details, the clear-sky albedo maps appear very consistent.

The all-sky albedo maps (Fig. 3) are dominated by the seasonally changing distributions of cloud cover, as for the all-sky LW flux (Fig. 1). Areas of bright high cloud over the monsoon areas in July are well observed; extended low-level marine clouds west of the continents, off Peru and Namibia, appear much more clearly than in the LW maps. Similarly the bright areas extending from southeast Asia over China to the northeast reveal the prevalence of low- and midlevel cloud.

c. Net flux

The net radiation (positive for input to the earth–atmosphere column) is the difference between the absorbed solar flux and the outgoing longwave flux:

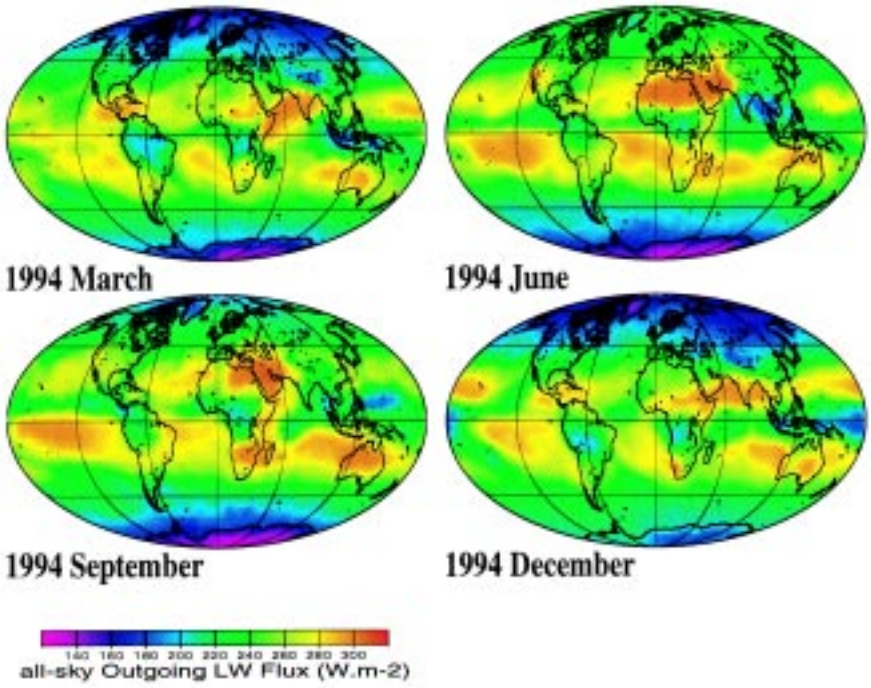

FIG. 1. Monthly means of the regional LW fluxes (all sky) determined with ScaRaB FM1 on *Meteor-3/7* from March, June, September, and December 1994.

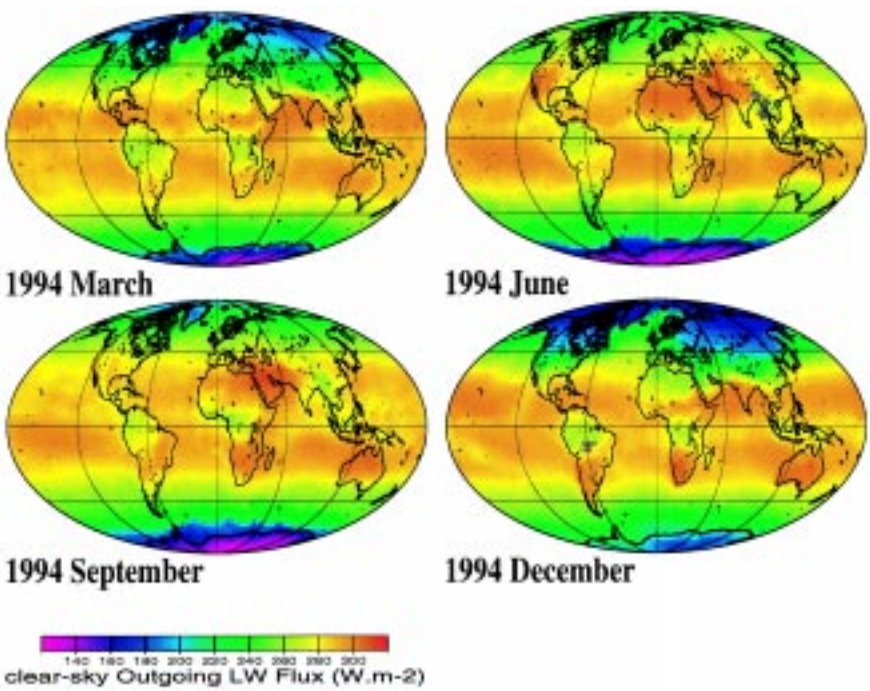

FIG. 2. Clear-sky regional LW fluxes; otherwise same as Fig. 1. Fluxes were interpolated through small no-data areas but not over extended ones (shown in gray).

$$R_n = M_{SW}^{inc}(1-\alpha) - M_{LW}^{em},$$

where α denotes the TOA albedo. Figure 5 shows the all-sky regional net flux averaged over the 11 months of ScaRaB. The heating zone ($R_n > 0$) is centered on the equator with maxima around 90 W m^{-2}, except in the eastern Pacific. Net flux is systematically negative at high latitudes; at low latitudes, anomalous negative values are observed over the deserts in Sahara and Arabia, and also over low stratiform clouds over both continents (western China) and oceans (off Peru, etc.). This annual (1994–95) mean geographical distribution of R_n is similar to those based on ERBE scanner data between 1985 and 1989. The annual global mean net radiative flux is found to be +2.5 W m^{-2}, closer to zero than found by ERBE (see Table 6). Such deviations from the nominal zero value are small compared to the range of uncertainty (cf. Kiehl and Trenberth 1997). They should not be interpreted as giving the value of climate change forcing (usually computed for the tropopause rather than TOA), but they are useful as a consistency test of the whole data processing. The annual cycle of global mean TOA ERB components and net radiation deduced from ScaRaB FM1 data is given in Table 6, together with a comparison of the ScaRaB and ERBE annual mean values. When calculating the annual means, the missing month (October 1994) has no significant impact because the near-equinox values of the ERB components are themselves very close to the annual mean. Note that larger uncertainties apply to ScaRaB values for near-terminator months (April, July, and November 1994, January 1995), especially for November 1994 for which the first 9 days are missing.

d. Comparison with ERBE results

As noted above, the annual global mean net radia-

tive flux found from the ScaRaB-1 observations is even closer to zero than the corresponding ERBE results. Examining the month-to-month variation of the global mean net (Fig. 6), we find that apart from a shift of 2.5 W m^{-2}, there is good agreement in shape between the ScaRaB variation and the 5 yr partially or completely observed by the ERBE scanner. The only ScaRaB point that appears somewhat discordant corresponds to November 1994, which as noted above is subject to greater uncertainties than other months; moreover, the spread of ERBE values (e.g., November 1985 vs November 1988) is the same. Comparable agreement is found in the annual cycles of the global and hemispheric means of LW and SW flux.

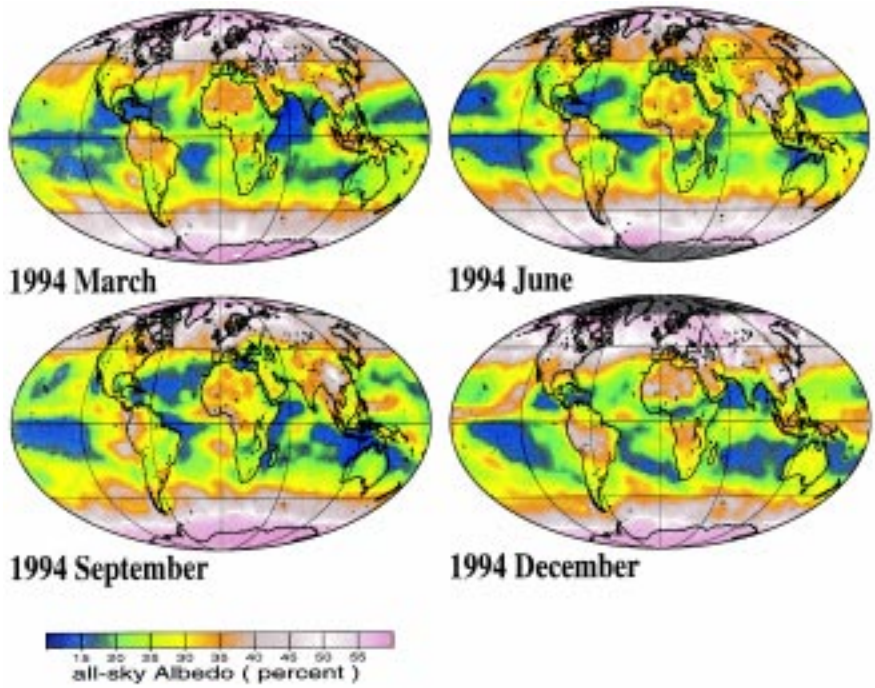

FIG. 3. All-sky regional albedo; otherwise same as Fig. 1.

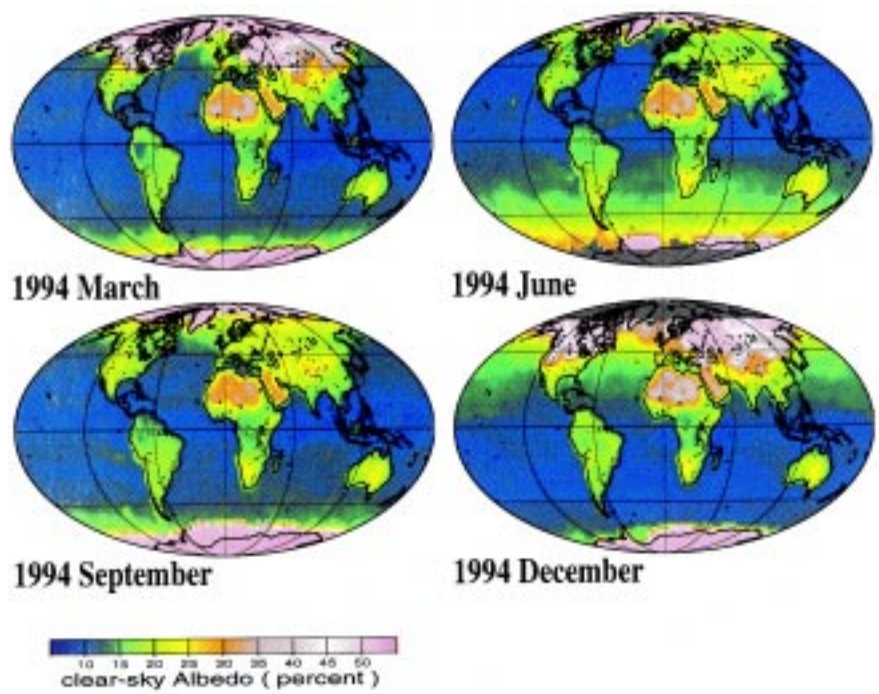

FIG. 4. Clear-sky albedos; otherwise as in Fig. 3.

Zonal mean values of both all-sky and clear-sky LW and SW fluxes are also in good agreement. In Fig. 7 we show the departures of the ScaRaB monthly zonal mean LW and SW fluxes for March, June, September, and December 1994 from the corresponding (4 or 5 yr) average ERBE scanner monthly zonal means. We also show the departures of the individual ERBE monthly zonal means for each of the 4 or 5 yr of available scanner data. The profile of the all-sky LW departure is shifted by about +2 W m^{-2} relative to ERBE (the vertical line of zero departure) and exhibits both positive and negative departures comparable in strength (±5 W m^{-2}) to those observed by ERBE for different years. For the all-sky SW, the ScaRaB shift is smaller. The overall spread of the ScaRaB departures is similar to that for the ERBE years. A departure greater than +20 W m^{-2} is observed near the South Pole in December 1994; however, the corresponding ERBE departures range from +10 (for December 1985 and 1986) to −10 W m^{-2} (for December 1987 and 1988). Also, near the North Pole, the July departures of ERBE values range from +18 to −12 W m^{-2}. Thus the SW spreads are similar. Near the poles, estimates of reflected SW flux are uncertain for both ERBE and ScaRaB. Cloud-ice discrimination is

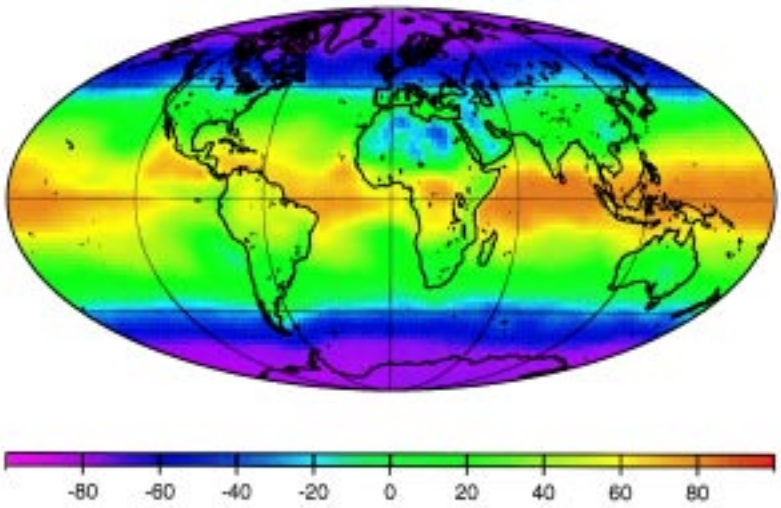

FIG. 5. Net radiation flux, averaged over 11 months from March 1994 to February 1995 (October 1994 missing).

uncertain, and scene identification errors are carried through into the mean fluxes by way of the angular corrections. Large departures also appear for both ScaRaB and ERBE clear-sky fluxes and albedos near the poles, but the average ScaRaB departure remains close to zero.

e. Cloud radiative forcing

The so-called CRF is defined as the difference between the clear-sky and all-sky radiation results (Charlock and Ramanathan 1985; Ramanathan et al. 1989). With a change of sign, CRF corresponds to the forcing that appears initially in a climate simulation that has been run to equilibrium *with* cloud–radiation interaction, when the model clouds are instantaneously rendered transparent to radiation (SW or LW or both).

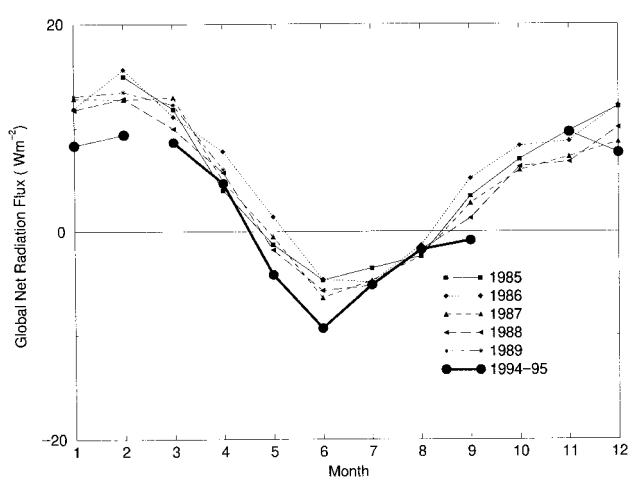

FIG. 6. Annual cycle of the global mean net radiation fluxes for the 5 ERBE yr and for ScaRaB.

Empirical evaluation of CRF may combine the rms errors of both all-sky and clear-sky quantities, so that the uncertainty may be as large as 10 W m^{-2} (Harrison et al. 1990). In addition, systematic errors in the SW or LW CRF may arise at various steps of the data processing, from the ground calibration (cf. Thomas et al. 1995) to the scene identification (Collins and Inamdar 1995; Ye and Coakley 1996; Stubenrauch et al. 1997), radiance-to-flux conversion, the angular and time sampling, and the time averaging, for which distinct (and possibly incorrect or unrepresentative) models are applied for clear and cloudy scenes. The LW CRF is positive (Table 6: global annual mean of order +30 W m^{-2})

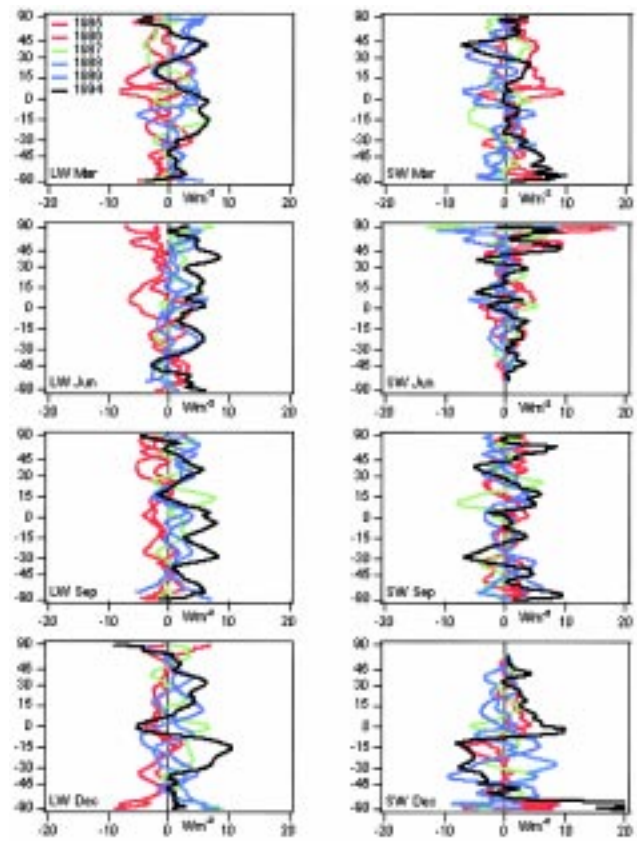

FIG. 7. Latitudinal profiles (ordinate marked in degrees, but with a sine latitude scale for equal-area weighting) of departures (in W m^{-2}) of ScaRaB zonal means of all-sky fluxes from the corresponding 4- or 5-yr averages of ERBE monthly zonal means. (left) Outgoing LW flux departures; (right) reflected SW. The months shown are March, June, September, and December, from top to bottom. Corresponding departure profiles for the individual ERBE scanner years are also shown.

since the clear-sky LW fluxes are generally higher than all-sky fluxes: thus clouds tend to warm the surface–atmosphere system and contribute to the natural greenhouse effect. The SW CRF is negative (global annual mean of order -50 W m^{-2}): clouds tend to cool the planet by blocking and returning directly to space a portion of the incident solar flux. Net CRF in the present climate (~ -20 W m^{-2}) appears to be a cooling effect.

Figure 8 shows the annual mean maps of LW, SW, and net CRF. Linear interpolations were used to fill in the missing clear-sky determinations in order to produce these maps. The strongest (positive) LW CRF values (up to 75 W m^{-2}) are associated with convective cloud in the ITCZ. Similarly, the strongest negative values of SW CRF are observed there. The net cloud radiative forcing is significantly negative over the globe as a whole, the strongest cooling (in blue) being observed over areas of persistent extended low clouds.

Just as was found for the annual global mean net radiative flux (previous section), the global annual averages of the LW, SW, and net CRF exhibit remarkable consistency between ScaRaB 1994 and ERBE 1985 (Table 6). Such results are striking, considering that the two experiments have different specific characteristics (instrument concept, calibration procedure, pixel size, time sampling, software independently developed). The intermediate parameters (scene identification, clear-sky fluxes, monthly mean fluxes, and CRF, etc.) and final results (global annual mean CRF) could be sensitive to these even though nearly the same (ERBE) algorithms were applied to the two datasets. Although similar biases (a few watts per square meter) may affect both ScaRaB and ERBE estimates of CRF, the agreement increases the confidence we can have in using such empirical estimates to reject many of the strongly discordant (tens of watts per square meter) model estimates of CRF (Cess et al., 1990). The agreement between global annual means should not lead us to ignore the often dramatic interannual differences observed on the regional scale (including such near-global-scale phenomena as ENSO events). Furthermore, although it does encourage us to believe that there are no significant discrepancies in calibration or in processing that would strongly bias the long-term (Nimbus/ERB–

TABLE 6. Annual cycle and averages of global means of ERB and CRF components.

Month	Flux (W m^{-2})			Albedo (percent)
	LW	SW	Net	
Mar 1994	234.9	102.0	+8.6	29.5
Apr 1994	234.7	100.3	+4.7	29.5
May 1994	238.1	100.6	–4.1	30.1
Jun 1994	241.5	99.4	–9.3	30.0
Jul 1994	240.7	96.8	–5.2	29.2
Aug 1994	241.2	94.0	–1.8	28.2
Sep 1994	241.4	97.6	–0.9	28.8
Oct 1994	—	—	—	—
Nov 1994	234.0	106.6	+9.5	30.5
Dec 1994	235.2	110.0	+7.6	31.1
Jan 1995	235.2	109.7	+8.3	31.1
Feb 1995	233.1	108.0	+9.3	30.8
Annual (11-month) means				
ScaRaB Mar 94–Feb 95	237.3	102.3	+2.4	29.9
ERBE Mar 85–Feb 86	234.1	101.9	+5.1	29.8
ERBE Mar 86–Feb 87	234.2	101.5	+5.5	29.7
ERBE Mar 87–Feb 88	236.3	100.8	+4.3	29.5
ERBE Mar 88–Feb 89	236.5	100.6	+4.2	29.5
ERBE Mar 85–Feb 89	235.3	101.2	+5.0	29.6
	LW CRF	**SW CRF**	**Net CRF**	
ERBE Mar 85–Feb 89	+29.1	–47.6	–18.5	
ScaRaB Mar 94–Feb 95	+27.2	–48.2	–21.0	

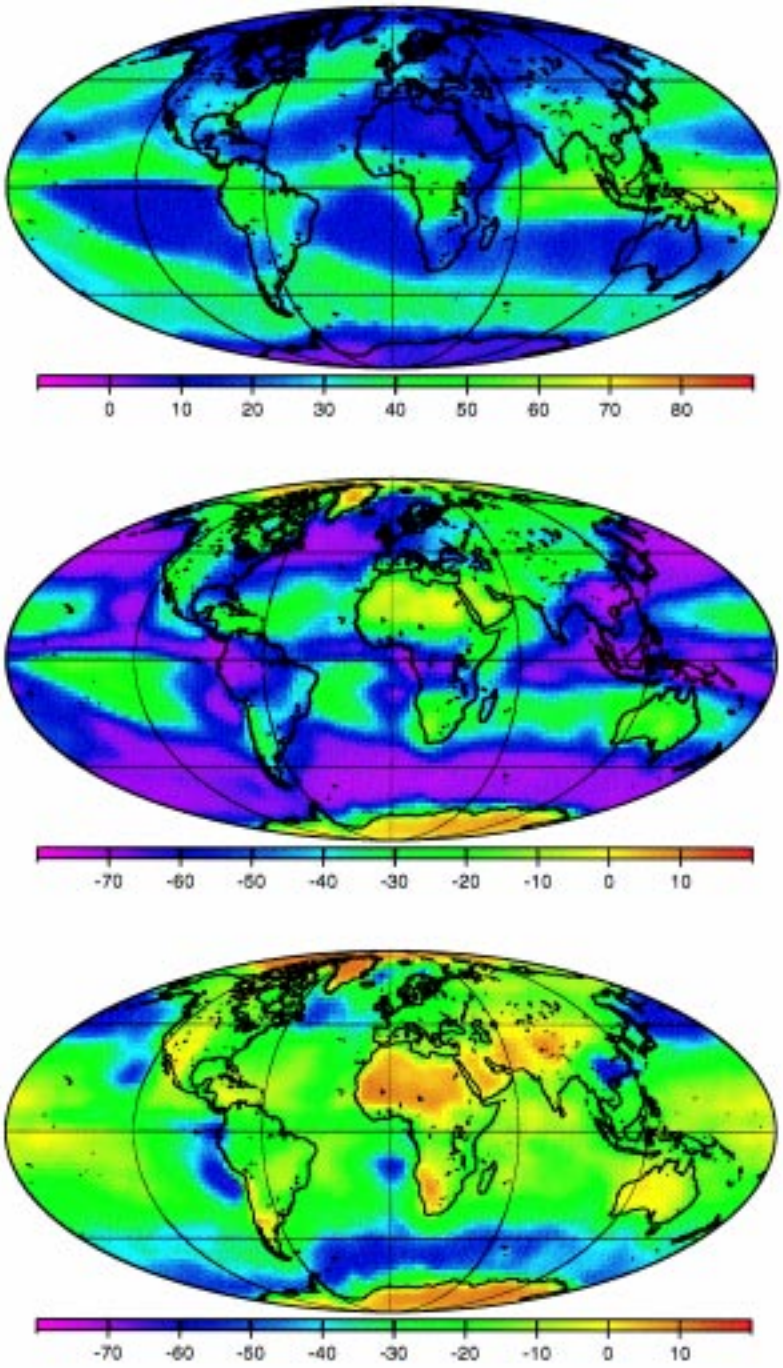

FIG. 8. Annual average regional values of the LW (top), SW (middle), and net (bottom) CRF from March 1994 to February 1995 (except October 1994). Linear interpolation was used to fill the missing clear-sky determinations in these maps.

ERBE–ScaRaB–CERES) record, this should not deter us from looking for processing improvements as outlined in section 4c in order to reduce bias and obtain better accuracy at smaller space and time scales, such as daily regional estimates.

6. Prospects for the coming years

We are now awaiting new broadband scanner observations from CERES on TRMM and ScaRaB FM2 on Ressurs, both to be launched in 1997–98, and launches of CERES on EOS-AM and -PM in 1998 and 2000 (Wielicki et al. 1996). Data from ScaRaB-2 on the polar orbiter Ressurs will be an invaluable complement to CERES/TRMM data, which will not extend above midlatitudes, and the combination will yield more complete time sampling in the tropical zone, allowing the validation and improvement of time interpolation procedures. The CERES scanners on board EOS-AM will be observing at roughly the same local times as ScaRaB/Ressurs, and this will provide opportunities for checking the accuracy of the ERB determinations.

The multiangular multichannel POLDER instrument (Polarization and Directionality of Reflectance; Deschamps et al. 1994) on board ADEOS, which unfortunately ceased operation in June 1997, has already provided data that will help to improve SW angular models. When ADEOS-2 is in operation, such data can be combined with near-simultaneous collocated views by the broadband scanners in operation, presumably after 1999. In coming years we also expect to develop improved algorithms for processing the existing ScaRaB-1 and expected ScaRaB-2 data. Work is in progress on adapting ISCCP (International Satellite Cloud Climatology Project) cloud detection algorithms to the coarse spatial resolution of the ScaRaB narrowband measurements so as to improve scene/cloud identification and thus clear-sky flux estimates. Similarly, ISCCP data products will be used for more realistic diurnal interpolation and time averaging (Haeffelin et al. 1998).

The ISSWG has judged that the first stage of validation of ERBE-like ScaRaB-1 data products is now complete. Note that, as stated for ERBE by Wielicki

and Green in 1989, "there is no direct way to validate the individual flux estimates. . . . Validation is achieved through the use of consistency checks, both theoretical and observational." We believe that further validation of the ScaRaB-1 products depends on further study in the broader scientific community, and it is the object of this paper to present the dataset to this community, without hiding the questions that may be raised regarding particular products. Scientific use of the ScaRaB-1 data has only begun. On average, considering the uncertainties in the measurements and processing algorithms, the 1994–95 TOA fluxes exhibit *no* change in global means and in their annual cycle when compared with corresponding ERBE values for the years 1985–90. Similarly, changes in zonal means remain within the range of interannual variability observed during the ERBE period. For the short period 1985–95, one would hardly expect to observe global change in the ERB components, and this observation of global invariance is a check on the consistency of ScaRaB calibration and data processing with ERBE. Global invariance has similarly been a check on procedures used to maintain uniformity in the long-term ISCCP dataset (Brest and Rossow 1992; Klein and Hartmann 1993). Such validations confirm that the often strong regional-scale (including Pacific Ocean–scale) changes observed in the ERB components are not instrumental or data processing artifacts. The year of ScaRaB-1 data and the expected ScaRaB-2 data are a valuable addition to the Nimbus/ERB–ERBE dataset.

Acknowledgments. We acknowledge the major contribution of the ScaRaB instrument designer, Jean-Louis Monge, and we salute the memory of the late Vladimir Adasko, chief constructor of the *Meteor-3* satellite. We also thank Francis Sirou (instrument project chief at LMD during the period of data analysis), Bernard Brioit, Alain Pellegrin, and Bernard Gillet at LMD, as well as the other engineers and technicians at Palaiseau (LMD), Orsay (IAS), Toulouse (CNES, INTESPACE), Moscow (Planeta/NITsIPR, RIEM), Istra (RIEM), Munich (Sensorlab), and at the solar ground calibration site at Izaña (Tenerife, Canary Islands) for their essential contributions to the success of this project. We also acknowledge the effective and difficult work of the rocket launch team at Plesetsk (Space Arm of Russia) and of the data reception and transmission teams at Obninsk, Moscow, and Toulouse. Important support and encouragement was provided at different moments at CNES (the French national space agency) by J.-L. Fellous, Ph. Waldteufel, A. Ratier, and N. Tabarié; at the Russian Hydrometeorological Service by V. F. Kharitonov and V. Karpov; and at DARA (the German space agency) by K.-D. Rockwitz. Also, we hope that the clarity of the paper was improved as a result of comments and suggestions of two anonymous reviewers.

References

Barkstrom, B. R., E. F. Harrison, G. L. Smith, R. Green, J. Kibler, R. Cess, and the ERBE Science Team, 1989: Earth Radiation Budget Experiment (ERBE) archival and April 1985 results. *Bull. Amer. Meteor. Soc.*, **70,** 1254–1262.

Bess, T. D., G. L. Smith, R. N. Green, D. A. Rutan, R. S. Kandel, P. Raberanto, and M. Viollier, 1997: Intercomparison of Scanning Radiometer for Radiation Budget (ScaRaB) and Earth Radiation Budget Experiment (ERBE) results. *Proc. Ninth Conf. Atmospheric Radiation,* Long Beach, CA, Amer. Meteor. Soc., 203–207.

Bony, S., and J.-P. Duvel, 1994: Influence of the vertical structure of the atmosphere on the seasonal variation of precipitable water and the greenhouse effect. *J. Geophys. Res.*, **99,** 12 963–12 980.

——, ——, and H. Le Treut, 1995: Observed dependence of the water vapor and clear-sky greenhouse effect on sea surface temperature. Comparison with climate warming experiments. *Climate Dyn.*, **11,** 307–320.

Brest, C. L., and W. B. Rossow, 1992: Radiometric calibration and monitoring of NOAA AVHRR data for ISCCP. *Int. J. Remote Sens.*, **13,** 235–273.

Briand, V., C. J. Stubenrauch, W. B. Rossow, A. Walker, and R. Holz, 1998: Scene identification for ScaRaB data: The ISCCP approach. *Satellite Remote Sensing of Clouds and the Atmosphere,* J. D. Haigh, Ed., SPIE, 242–252.

Brooks, D. R., E. H. Harrison, P. Minnis, J. T. Suttles, and R. Kandel, 1986: Development of algorithms for understanding the temporal and spatial variability of the Earth's Radiation Balance. *Rev. Geophys.*, **24,** 422–438.

Capderou, M., 1995: Une année de ScaRaB. Orbitographie et échantillonnage temporel pour le satellite Meteor-3/07. ScaRaB (février 1994–mars 1995). LMD Note Technique 199, 250 pp. [Available from LMD, Ecole Polytechnique, F-91128 Palaiseau Cedex, France.]

——, 1997: Determination of the shortwave anisotropic function for clear-sky desert scenes from ScaRaB data; comparison with results obtained from Sunsynchronous and geosynchronous satellite data. *IRS '96: Current Problems in Atmospheric Radiation,* W. L. Smith and K. Stamnes, Eds., A. Deepak Publishing, 766–769.

Cess, R. D., and G. L. Potter, 1987: Exploratory studies of cloud radiative forcing with a general circulation model. *Tellus,* **39A,** 460–473.

——, and Coauthors, 1990: Intercomparison and interpretation of climate feedback processes in 19 atmospheric general circulation models. *J. Geophys. Res.*, **95,** 16 601–16 615.

Charlock, T. P., and V. Ramanathan, 1985: The albedo field and cloud radiative forcing produced by a general circulation model with internally generated cloud optics. *J. Atmos. Sci.*, **42,** 1408–1429.

Cheruy, F., R. S. Kandel, and J. P. Duvel, 1991: Outgoing longwave radiation and its diurnal variation from combined ERBE and Meteosat observations. Part II: Using Meteosat data to determine the LW diurnal cycle. *J. Geophys. Res.*, **96,** 22 623–22 630.

Collins, W. D., and A. K. Inamdar, 1995: Validation of clear-sky fluxes for tropical oceans from the Earth Radiation Budget Experiment. *J. Climate,* **8,** 569–578.

Deschamps, P.-Y., F.-M. Bréon, M. Leroy, A. Podaire, A. Bricaud, J.-C. Buriez, and G. Sèze, 1994: The POLDER mission: Instrument characteristics and scientific objectives. *IEEE Trans. Geosci. Remote Sens.,* **32,** 598–615.

Dinguirard, M., and T. Trémas, 1997: Project ScaRaB: Bilan radiométrique en vol du MV1. CNES Document CT/IA/QTIS/GC 97-172. 39 pp. [Available from Centre National d'Etudes Spatiales, 18 avenue Edouard Belin, F-31401 Toulouse, Cedex 4, France.]

Doelling, D. R., L. Nguyen, W. L. Smith Jr., and P. Minnis, 1998: Comparison of ARM GOES-derived broadband fluxes and albedoes with broadband data from ARM-UAV, ScaRaB, and CERES. *Proc. Eighth ARM Science Team Meeting,* Tuscon, AZ, in press.

Duvel, J. P., 1988: Analysis of diurnal, interdiurnal and interannual variation during Northern Hemisphere summers using Meteosat Infrared channels. *J. Climate,* **1,** 471–484.

——, and R. Kandel, 1985: Regional-scale diurnal variations of outgoing radiation observed by Meteosat. *J. Climate Appl. Meteor.,* **24,** 335–349.

Green, R. N., and L. M. Avis, 1996: Validation of ERBS scanner radiances. *J. Atmos. Oceanic Technol.,* **13,** 851–862.

——, F. B. House, P. W. Stackhouse, X. Wu, S. A. Ackerman, W. L. Smith, and M. J. Johnson, 1990: Intercomparison of scanner and nonscanner measurements for the Earth Radiation Budget Experiment. *J. Geophys. Res.,* **95,** 11 785–11 798.

Haeffelin, M., R. Kandel, and C. Stubenrauch, 1998: Improved diurnal interpolation of reflected broadband shortwave observations using ISCCP data. *J. Atmos. Oceanic Technol.,* in press.

Harrison, E. F., P. Minnis, B. R. Barkstrom, V. Ramanathan, R. D. Cess, and G. G. Gibson, 1990: Seasonal variation of cloud radiative forcing derived from the Earth Radiation Budget Experiment. *J. Geophys. Res.,* **95,** 18 687–18 703.

House, F. B., A. Gruber, G. E. Hunt, and A. T. Mecherikunnel, 1986: History of satellite missions and measurements of the Earth Radiation Budget. *Rev. Geophys.,* **24,** 357–377.

Hunt, G. E., R. S. Kandel, and A. T. Mecherikunnel, 1986: A history of presatellite investigations of the Earth's Radiation Budget. *Rev. Geophys.,* **24,** 351–356.

Jacobowitz, H., H. V. Soule, H. L. Kyle, F. B. House, and the *Nimbus-7* ERB Experiment Team, 1984: The Earth Radiation Budget (ERB) experiment: An overview. *J. Geophys. Res.,* **89,** 5021–5038.

Kandel, R. S., 1990: Satellite observations of the Earth Radiation Budget and clouds. *Space Sci. Rev.,* **52,** 1–32.

——, J.-L. Monge, M. Viollier, L. A. Pakhomov, V. I. Adasko, R. G. Reitenbach, E. Raschke, and R. Stuhlmann, 1994a: The ScaRaB project: Earth radiation budget observations from the Meteor satellites, World Space Congress (Washington, 1992)—COSPAR Symp. A.2-S. *Adv. Space Res.,* **14,** 147–154.

——, D. Thomas, and J. Ph. Duvel, 1994b: Earth Radiation Budget observation from geostationary satellites. *Proc. 10th Meteosat Scientific Users' Meeting,* Cascais, Portugal, 327–335.

Kiehl, J. T., and K. E. Trenberth, 1997: Earth's annual global mean energy budget. *Bull. Amer. Meteor. Soc.,* **78,** 197–208.

Klein, S. A., and D. L. Hartmann, 1993: Spurious changes in the ISCCP dataset. *Geophys. Res. Lett.,* **20,** 455–458.

Li, Z., and A. Trishchenko, 1998: A study toward a better understanding of the relation between visible and SW measurements. *J. Atmos. Oceanic Technol.,* in press.

Minnis, P., E. F. Harrison, L. L. Stowe, G. G. Gibson, F. M. Denn, D. R. Doelling, and W. L. Smith Jr., 1993: Radiative climate forcing by the Mt. Pinatubo eruption. *Science,* **259,** 1411–1415.

Monge, J. L., R. S. Kandel, L. A. Pakhomov, and V. I. Adasko, 1991: ScaRaB earth radiation budget scanning radiometer. *Metrologia,* **28,** 261–284.

Mueller, J., R. Stuhlmann, E. Raschke, J. L. Monge, R. Kandel, P. Burkert, and L. A. Pakhomov, 1993: Solar ground calibration of ScaRaB preliminary results. *Passive Infrared Remote Sensing of Clouds and the Atmosphere,* D. K. Lynch, Ed., SPIE, 129–139.

——, ——, R. Becker, E. Raschke, J.-L. Monge, and P. Burkert, 1996: Ground-based calibration facility for the Scanner for Radiation Budget instrument in the solar spectral domain. *Metrologia,* **32,** 657–660.

——, and Coauthors, 1997: Ground characterization of the Scanner for Radiation Budget (ScaRaB) Flight Model 1. *J. Atmos. Oceanic Technol.,* **14,** 802–813.

Raison, F., 1996: Modélisation et étude du bilan radiométrique de l'instrument ScaRaB embarqué sur le satellite Météor-3/7. Thèse, Université de Paris VII (Denis Diderot), 197 pp. [Available from LMD, Ecole Polytechnique, F-91128 Palaiseau Cedex, France.]

——, and R. Kandel, 1995: Verifying shortwave in-flight calibration of the ScaRaB/Meteor radiation budget scanner. *Passive Infrared Remote Sensing of Clouds and the Atmosphere,* D. K. Lynch, Ed., SPIE, 367–374.

Ramanathan, V., R. D. Cess, E. F. Harrison, P. Minnis, B. R. Barkstrom, E. Ahmad, and D. Hartmann, 1989: Cloud-radiative forcing and climate: Results from the Earth Radiation Budget Experiment. *Science,* **243,** 57–63.

Raschke, E., T. H. Vonder Haar, W. R. Bandeen, and M. Pasternak, 1973: The annual radiation balance of the earth–atmosphere system during 1969–1970 from *Nimbus-3* measurements. *J. Atmos. Sci.,* **30,** 341–364.

Raval, A., and V. Ramanathan, 1989: Observational determination of the greenhouse effect. *Nature,* **342,** 758–761.

Rieland, M., and E. Raschke, 1991: Diurnal variability of the Earth radiation budget: Sampling requirements, time integration aspects, and error estimates for the Earth Radiation Budget Experiment (ERBE). *Theor. Appl. Climatol.,* **44,** 9–24.

Smith, G. L., R. N. Green, E. Raschke, L. M. Avis, J. T. Suttles, B. A. Wielicki, and R. Davies, 1986: Inversion methods for satellite studies of the earth's radiation budget: Development of algorithms for the ERBE mission. *Rev. Geophys.,* **24,** 407–421.

Sohn, B. J., and F. R. Robertson, 1993: Intercomparison of observed cloud radiative forcing: A zonal and global perspective. *Bull. Amer. Meteor. Soc.,* **74,** 997–1006.

Standfuss, C., 1997: Synergie von satellitendaten am beispiel der modellierung des tagesganges der planetaren strahlungsbilanz. GKSS Rep. 97/E/24, 103 pp. [Available from GKSS Forschungszentrum Geesthacht, Bibliothek, Postfach 1160, D-21494 Geesthacht, Germany.]

Stephens, G. L., and T. J. Greenwald, 1991a: The Earth's Radiation Budget and its relation to atmospheric hydrology 1. Observations of the clear sky greenhouse effect. *J. Geophys. Res.,* **96,** 15 311–15 324.

——, and ——, 1991b: The Earth's Radiation Budget and its relation to atmospheric hydrology 2. Observations of cloud effect. *J. Geophys. Res.,* **96,** 15 325–15 340.

——, G. G. Campbell, and T. H. Vonder Haar, 1981: Earth radiation budgets measurements from satellites and their interpretation for climate modeling and studies. *J. Geophys. Res.,* **86,** 9739–9760.

Stowe, L. L., Ed., 1988: Report of the Earth Radiation Budget Requirements Review—1987, NOAA Tech. Rep. NESDIS-41, 103 pp.

Stubenrauch, C., J.-P. Duvel, and R. S. Kandel, 1993: Determination of longwave anisotropic emission factors from combined broad- and narrowband radiance measurements. *J. Appl. Meteor.,* **32,** 848–856.

——, A. D. Del Genio, and W. B. Rossow, 1997: Implementation of subgrid cloud vertical structure inside a GCM and its effect on the radiation budget. *J. Climate,* **10**, 273–287.

Suttles, J. T., and Coauthors, 1988a: *Angular Radiation Models for the Earth–Atmosphere System.* Vol. 1. NASA, 147 pp.

——, R. N. Green, G. L. Smith, B. A. Wielicki, I. J. Walker, V. R. Taylor, and L. L. Stowe, 1988b: *Angular Radiation Models for the Earth–Atmosphere System.* Vol. II. NASA, 87 pp.

——, B. A. Wielicki, and S. Vemury, 1992: Top-of-atmosphere radiative fluxes: Validation of ERBE scanner inversion using *Nimbus-7* ERB data. *J. Appl. Meteor.,* **31,** 784–796.

Thomas, D., J.-P. Duvel, and R. Kandel, 1995: Diurnal bias in calibration of broad-band radiance measurements from space. *IEEE Trans. Geosci. Remote Sens.,* **33,** 670–683.

Trenberth, K. E., and T. J. Hoar, 1996: The 1990–1995 El Niño–Southern Oscillation event: Longest on record. *Geophys. Res. Lett.,* **23,** 57–60.

Trishchenko, A., and Z. Li, 1998: Use of ScaRaB measurements for validating a GOES-based TOA radiation product. *J. Appl. Meteor.,* in press.

Viollier, M., R. Kandel, and P. Raberanto, 1995: Inversion and space-time averaging algorithms for ScaRaB (Scanner for Earth Radiation Budget)—Comparison with ERBE. *Ann. Geophys.,* **13,** 959–968.

——, ——, ——, M. Dejmek, and S. Teshigawara, 1997: Overview of one year of ScaRaB data with regard to the effects of restricted time sampling. *IRS'96: Current Problems in Atmospheric Radiation,* W. L. Smith and K. Stamnes, Eds., A. Deepak Publishing, 790–793.

Wessel, P., and W. H. F. Smith, 1991: Free software helps map and display data. *Eos, Trans. Amer. Geophys. Union,* **72,** 445–446.

Wielicki, B. A., and R. N. Green, 1989: Cloud identification for ERBE radiative flux retrieval. *J. Appl. Meteor.,* **28,** 1133–1146.

——, and Coauthors, 1995: Mission to Planet Earth: Role of clouds and radiation in climate. *Bull. Amer. Meteor. Soc.,* **76,** 2125–2153.

——, and Coauthors, 1996: Clouds and the Earth's Radiant Energy System (CERES): An Earth Observing System experiment. *Bull. Amer. Meteor. Soc.,* **77,** 853–868.

Ye, Q., and J. A. Coakley Jr., 1996: Biases in Earth Radiation Budget observations. 2. Consistent scene identification and anisotropic factors. *J. Geophys. Res.,* **101,** 21 253–21 263.